Navigated Self-Assembly of a Pd2L4 Cage by Modulation of an Energy Landscape under Kinetic Control

Navigated Self-Assembly of a Pd_2L_4 Cage by Modulation of an Energy Landscape under Kinetic Control

Tomoki Tateishi,[1] Satoshi Takahashi,[1] Atsushi Okazawa,[1] Vicente Martí-Centelles,[2] Jianzhu Wang,[2] Tatsuo Kojima,[1] Paul J. Lusby,[2,*] Hirofumi Sato,[3,4,5] and Shuichi Hiraoka[1,*]

[1]Department of Basic Science, Graduate School of Arts and Sciences, The University of Tokyo, 3-8-1 Komaba, Meguro-ku, Tokyo 153-8902, Japan

[2]EaStCHEM School of Chemistry, University of Edinburgh, Joseph Black Building, David Brewster Road, Edinburgh, Scotland EH9 3FJ, UK

[3]Department of Molecular Engineering, Kyoto University, Kyoto 615-8510, Japan

[4]Elements Strategy Initiative for Catalysts and Batteries, Kyoto University, Kyoto 615-8510, Japan

[5]Fukui Institute for Fundamental Chemistry, Kyoto University, Kyoto 606-8103, Japan

ABSTRACT: Kinetic control of molecular self-assembly remains difficult because of insufficient understanding of molecular self-assembly mechanism. Here we report the formation of a metastable $[Pd_2L_4]^{4+}$ cage structure composed of naphthalene-based ditopic ligands (L) and Pd(II) ions in very high yield (99%) under kinetic control by modulating the energy landscape. The guest anion trapped in the cage and the solvent with very weak coordination ability prefer the formation of suitable intermediates and prevent the conversion of the metastable cage into the thermodynamically most stable decomposed state. The cage formation pathways under kinetic control and the effect of the anions encapsulated on the self-assembly processes were investigated by QASAP (quantitative analysis of self-assembly process) and NASAP (numerical analysis of self-assembly process). It was found that the self-assembly with a preferred guest (BF_4^-) proceeds through intermediates composed of no more components than the cage ($[Pd_aL_bX_c]^{2a+}$ ($a \leq 2$, $b \leq 4$, X indicates a leaving ligand)) and that the final intramolecular cage-closure step is the rate-determining step. In contrast, a weaker guest (OTf^-) causes the transient formation of intermediates composed of more components than the cage ($[Pd_aL_bX_c]^{2a+}$ ($a > 2$, $b > 4$)), which are finally converted into the cage.

INTRODUCTION

Controlling molecular self-assembly to bias the production of a desired assembled structure depends on nature of the product. If the desired structure is thermodynamically most stable, the reaction conditions should be selected so that the self-assembly can easily reach equilibration. If the desired structure is not thermodynamically most stable, isolating the product depends on modulating the reaction conditions to select a given reaction pathway on the energy landscape so as to avoid the thermodynamic sink and efficiently produce the metastable state. In many cases, molecular self-assemblies proceed under thermodynamic control based on reversible chemical bonds connecting the building blocks,[1] so self-assembly pathways have tended to be disregarded.[2] However, an understanding of molecular self-assembly processes enables selected metastable species to be produced under kinetic control along a well-defined pathway, which is created by modulating the energy landscape.[3]

Here we report an example of kinetically controlled molecular self-assembly found in a Pd_2L_4 cage system.[4] The self-assembly from ditopic ligands **1** and Pd(II) ions in the absence of a guest molecule leads to a complex mixture containing 40-nm-sized large species as major species, because the $[Pd_2\mathbf{1}_4]^{4+}$ cage is likely to be destabilized by electrostatic repulsion between the two Pd(II) ions with a short separation (Figure 1). In the presence of a guest anion (Y^-), however, the self-assembly smoothly proceeds at 298 K to produce a $(Y^-)\subset[Pd_2\mathbf{1}_4]^{4+}$ cage, where the guest anion (Y^-) is encapsulated in the cavity of the $[Pd_2\mathbf{1}_4]^{4+}$ cage. The cage is not thermodynamically most stable but metastable at 298 K because heating of a solution of the cage causes its decomposition. Thus, the self-assembly of the $(Y^-)\subset[Pd_2\mathbf{1}_4]^{4+}$ cage is disadvantageous in such solvents that promote ligand exchanges by their coordination to the Pd(II) centers. Consequently, the metastable $(Y^-)\subset[Pd_2\mathbf{1}_4]^{4+}$ cage was obtained in very high yield (99%) under optimized reaction conditions (in the presence of BF_4^- in weak coordinative solvent CD_3NO_2). The navigated self-assembly process was analyzed experimentally (QASAP: quantitative analysis of self-assembly process)[5] and numerically (NASAP: numerical analysis of self-assembly process)[2g,6] to reveal the effect of guest anions on the energy landscape. QASAP indicates that a good guest anion (BF_4^-) promotes the formation of a partial cage structure, $(Y^-)\subset[Pd_2\mathbf{1}_4X]^{4+}$ (X indicates a leaving ligand). The conversion of the partial cage structure to the cage is the rate-determining step, which was supported by NASAP. With OTf^- counter anion, which is encapsulated more weakly than BF_4^-, the cage is formed through intermediates consisting of more components than the cage, $[Pd_a\mathbf{1}_bX_c]^{2a+}$ ($a > 2$, $b > 4$). The metastable $(Y^-)\subset[Pd_2\mathbf{1}_4]^{4+}$ cages, which cannot be obtained under usual

conditions of Pd(II)-linked coordination self-assemblies (in coordinative solvent at high temperature), are produced almost quantitatively by modulation of the energy landscape.

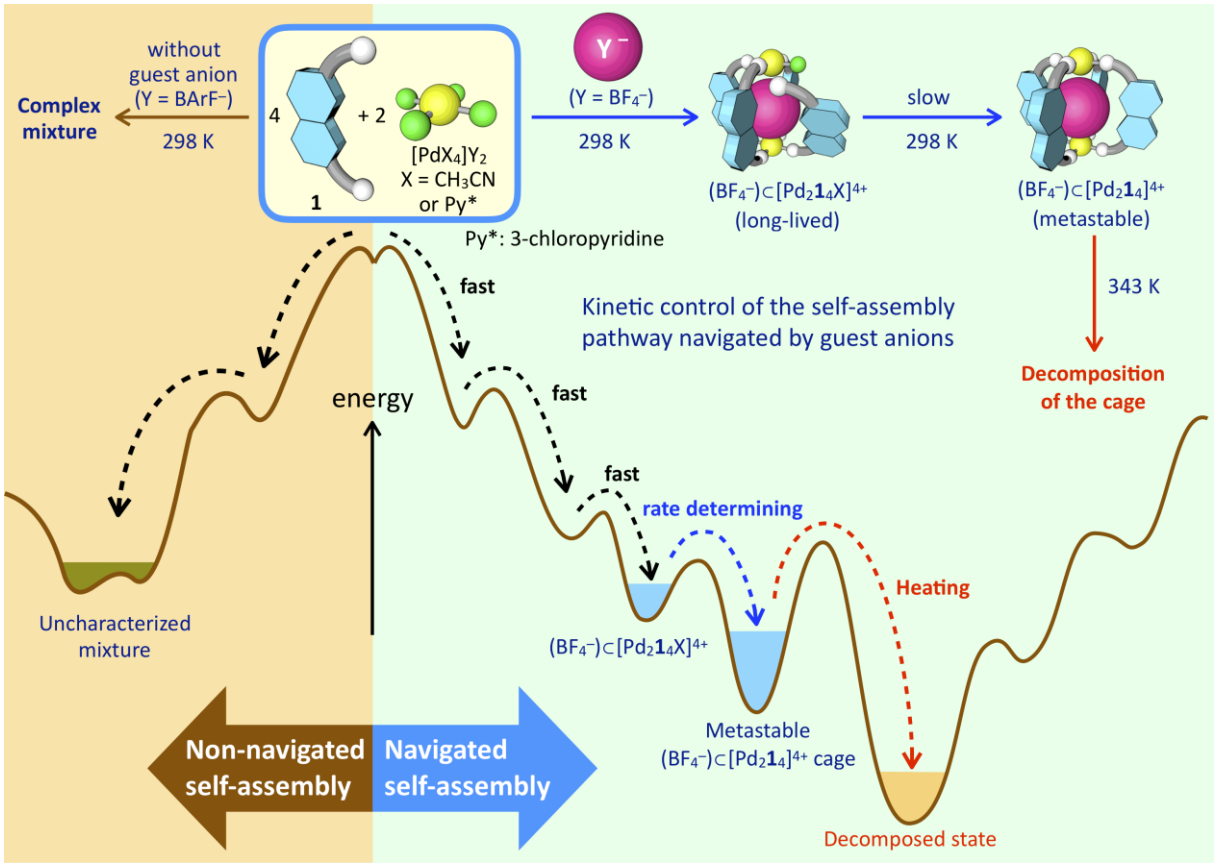

Figure 1. Navigated self-assembly of the $(BF_4^-)\subset[Pd_2\mathbf{1}_4]^{4+}$ cage from ditopic ligands **1** and $[PdX_4]Y_2$ (X = CH_3CN or Py*, Y = BF_4 or BArF). The chemical structures of **1** and Py* are shown in Figure 3. In the absence of guest anions, the self-assembly gave a complex mixture containing 40-nm-sized large species and the $[Pd_2\mathbf{1}_4]^{4+}$ cage (24% at most), while the $(BF_4^-)\subset[Pd_2\mathbf{1}_4]^{4+}$ cage was obtained in very high yield in the presence of a guest anion with high binding affinity, which modulates the energy landscape of the self-assembly so that suitable intermediates for the cage are efficiently generated during the self-assembly. When the self-assembly was carried out at high temperature (343 K) in solvent with coordination ability (CD_3CN or DMSO-d_6), the coordination bonds in the cage were recombined to result in the thermodynamically most stable decomposed state.

RESULTS AND DISCUSSION

Ditopic ligand **1** (Figure 2), where two 3-pyridyl rings are introduced in a naphthalene ring, was designed to give a Pd_2L_4 host for small, organic ditopic guests, building on the encapsulation methodology developed by the Lusby group.[7] A molecular modeling study of the $[Pd_2\mathbf{1}_4]^{4+}$ cage shows that there is not significant structural distortion in the ditopic ligands and around the Pd(II) centers of the cage, suggesting that this cage seems to be enthalpically stable enough to be produced under usual conditions adopted in coordination self-assembly. Besides, since this ligand is relatively rigid, the entropic loss for the formation of the $[Pd_2\mathbf{1}_4]^{4+}$ cage would be small, which is also advantageous to produce the cage under thermodynamic control. However, the self-assembly from **1** and $[Pd(CH_3CN)_4]Y_2$ (Y = BF_4 or OTf) in CD_3CN and CD_2Cl_2 (4:1, v/v) at 343 K for 14 h gave the cage in lower yields than expected: 51% (Y = BF_4) and 60% (Y = OTf), which were determined by ^{1}H NMR spectroscopy using an internal standard. CD_2Cl_2 was added because of slightly low solubility of **1** in polar solvent. If kinetically trapped species are produced during the self-assembly, these species would be converted into the cage in more coordinating solvents, which promote ligand exchanges to correct "wrong" connections.[8] Thus, the self-assembly from **1** and $[Pd(CH_3CN)_4](BF_4)_2$ was carried out in DMSO-d_6 and CD_2Cl_2 (4:1, v/v) at 343 K for 12 h but surprisingly the cage was not obtained at all. Then, the self-assembly in DMSO-d_6 and CD_2Cl_2 (4:1, v/v) was monitored by ^{1}H NMR spectroscopy. It was found that the yield of the cage reached 86% at 30 min, after which the yield decreased with time to finally reached 0% at 12 h (Figure S1a). This result suggests that the $[Pd_2\mathbf{1}_4]^{4+}$ cage is not thermodynamically most stable, yet metastable. The self-assembly of the cage in CD_3CN and CD_2Cl_2 (4:1, v/v) at 343 K was also monitored by ^{1}H NMR spectroscopy. As observed in DMSO-d_6, most of the cages were decomposed by heating in CD_3CN, though the decomposition in CD_3CN is slower than in DMSO-d_6 (Figure S1b and c). Heating the reaction mixture in CD_3CN gave a precipitate, suggesting the formation of insoluble polymeric structures. The precipitate was not found by heating in DMSO-d_6, probably because the polymeric, or oligomeric, structures are soluble in more polar solvent DMSO-d_6. These results suggest that more coordinative solvent promotes the decomposition of the cage faster by the initiating the rearrangement of the Pd(II)–N coordination bonds in the cage to

lead to thermodynamically more stable species than the cage. Prominent signals for the thermodynamic product(s) were not observed by ^{1}H NMR spectroscopy after the decomposition of the cage, and ESI-TOF mass spectrometry of the reaction mixture did not show any species larger than the cage (Figure S1d).

Since coordinating solvents tended to decompose the cage, CD_3NO_2, whose coordination ability is much weaker than either CD_3CN or DMSO-d_6, was used as the major solvent. When the self-assembly of the cage was carried out from **1** and $[Pd(CH_3CN)_4](OTf)_2$ in CD_3NO_2 and CD_2Cl_2 (4:1, v/v) at 343 K, the yield of the cage was 62%, which is almost the same as the yield obtained in CD_3CN (60%). However, the decomposition of the cage was largely suppressed in CD_3NO_2. Surprisingly, the self-assembly from **1** and $[Pd(CH_3CN)_4](BF_4)_2$ at 343 K gave the cage in 99% yield. This result suggests that the self-assembly of the $[Pd_2\mathbf{1}_4]^{4+}$ cage is strongly affected not only by solvents but also by counter anions.

The encapsulation of the counter anions (BF_4^- or OTf^-) in the cavity of the cage was confirmed by ^{19}F NMR spectroscopy (Figure S2). Two ^{19}F NMR signals for the encapsulated and free anions were observed, indicating the exchange of the free and bound anions is slower than the NMR timescale. Their integrations indicate that one counter anion is encapsulated in the $[Pd_2\mathbf{1}_4]^{4+}$ cage. The inclusion complexes, $(Y^-)\subset[Pd_2\mathbf{1}_4]^{4+}$ (Y = BF_4 and OTf), were further characterized by ^{1}H-^{19}F NOESY and ^{1}H and ^{19}F DOSY spectroscopies. The correlation between the ^{19}F NMR signal of the encapsulated BF_4^- and the ^{1}H NMR signals for the hydrogen atoms inside the cavity (H^a and H^g) was observed (Figure S3). The diffusion coefficient of the ^{19}F NMR signal of the encapsulated OTf^-, 6.51×10^{-10} m^2 s^{-1}, is similar to that of the ^{1}H NMR signals of the cage, 6.49×10^{-10} m^2 s^{-1} (Figures S4 and S5). The encapsulation of BF_4^- in the cage was also confirmed in the same way (Figures S3 and S5).

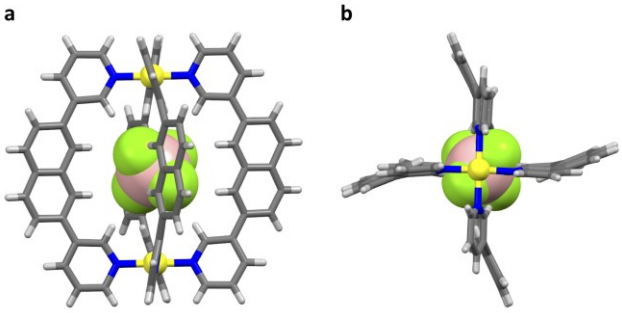

Figure 2. Crystal structure of the $(BF_4^-)\subset[Pd_2\mathbf{1}_4]^{4+}$ cage. (a) A side view. (b) A top view. The $[Pd_2\mathbf{1}_4]^{4+}$ cage is shown as a stick model, while the encapsulated BF_4^- is shown as a CPK model. One configuration is shown for the disordered BF_4^- anion. Color labels: grey, C; white, H; yellow, Pd; blue, N; pink, B; green, F.

Finally, the structure of the $(BF_4^-)\subset[Pd_2\mathbf{1}_4]^{4+}$ cage was revealed by single-crystal X-ray analysis. Single crystals of the cage were obtained by diffusion of benzene in a solution of the cage in CH_3NO_2 at 298 K for 7 weeks. Four ditopic ligands, **1**, are connected by two Pd(II) ions with a square-planar coordination geometry to form an 1-nm-sized cage structure, where the ditopic ligands **1** are slightly distorted (Figures 2 and S6). There are two crystallographically independent cage in the unit cell, and the intramolecular distances between the two Pd(II) ions are 9.789 and 9.808 Å. One BF_4^- anion is encapsulated in the cavity of the cage, being placed in a disordered manner at the inversion center of site symmetry between the two Pd(II) ions. Some short F···H^a and F···H^g contacts are found between the guest BF_4^- and **1** of the host cage, where the respective shortest distances of 2.627 and 2.587 Å are apparently shorter than the sum of their van der Waals radii (2.670 Å), suggesting a strong host–guest interaction. The average value of the shortest distances between each fluorine atom and H^g is 2.643 Å (H^a: 2.691 Å), which implies that the BF_4^- anion just fits into the cavity. These results are consistent with the solution structure of the $(BF_4^-)\subset[Pd_2\mathbf{1}_4]^{4+}$ cage.

The relative binding affinity between OTf^- and BF_4^- for the cage was investigated by competition experiments. Upon addition of *n*-Bu_4NBF_4 to a solution of $(OTf^-)\subset[Pd_2\mathbf{1}_4]^{4+}$, most of the OTf^- anions in the cage were exchanged with BF_4^- to give the $(BF_4^-)\subset[Pd_2\mathbf{1}_4]^{4+}$ cage, while nothing happened by addition of *n*-Bu_4NOTf to a solution of $(BF_4^-)\subset[Pd_2\mathbf{1}_4]^{4+}$ (Figure S7). These results indicate that BF_4^- is a stronger guest for the $[Pd_2\mathbf{1}_4]^{4+}$ cage. As the yield of the cage from $[Pd(CH_3CN)_4](BF_4)_2$, 99%, is much higher than that from $[Pd(CH_3CN)_4](OTf)_2$, 62%, the guest with higher binding affinity (BF_4^-) assists the self-assembly of the cage more efficiently.

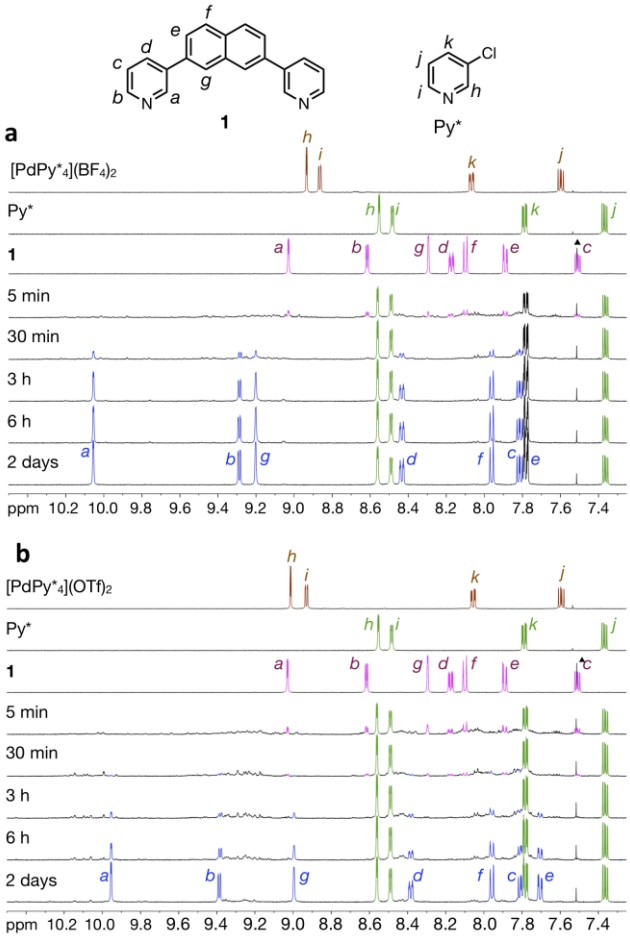

Figure 3. ^{1}H NMR spectra (500 MHz, aromatic region, 298 K) of $[PdPy^*_4]Y_2$ and Py* in CD_3NO_2 and **1** and the reaction mixture for the self-assembly of the $(Y^-)\subset[Pd_2\mathbf{1}_4]^{4+}$ cage from $[PdPy^*_4]Y_2$ in CD_3NO_2 and CD_2Cl_2 (4:1, v/v) at 298 K. (a) The self-assembly from $[PdPy^*_4](BF_4)_2$ ([Pd] = 0.95 mM) and **1** ($[\mathbf{1}]_0$ = 1.9 mM). (b) The self-assembly from $[PdPy^*_4](OTf)_2$ ([Pd] = 0.90 mM) and **1** ($[\mathbf{1}]_0$ = 1.8 mM). The signals colored in blue, green, magenta, and brown indicate the $(Y^-)\subset[Pd_2\mathbf{1}_4]^{4+}$ cage, Py*, **1**, and $[PdPy^*_4]Y_2$, respectively. The signal at 7.78 ppm in (a) was not colored because

the H^k signal of Py* and the H^e signal of the $(BF_4^-)\subset[Pd_2\mathbf{1}_4]^{4+}$ cage are overlapped. The signal marked with the black solid triangle at 7.52 ppm indicates $CHCl_3$, which was used during the preparation of the reaction mixture.

The effect of counter anions on the self-assembly process of the cage was investigated by QASAP.[5] QASAP is a method to find transiently produced intermediates, most of which cannot be observed by spectroscopy, by quantifying all the substrates and the products. In the case of the self-assembly of the $(Y^-)\subset[Pd_2\mathbf{1}_4]^{4+}$ cage from **1** and $[PdX_4]Y_2$ (X and Y indicate a leaving ligand and counter anion, respectively), any intermediate in this self-assembly can be expressed as $[Pd_a\mathbf{1}_bX_c]^{2a+}$ ($a - c$ indicate the number of components). From the amount of the substrates (**1** and $[PdX_4]Y_2$) and the products ($(Y^-)\subset[Pd_2\mathbf{1}_4]^{4+}$ and X) at given time, the average composition of all the intermediates, which can be expressed as $[Pd_{\langle a\rangle}\mathbf{1}_{\langle b\rangle}X_{\langle c\rangle}]^{2\langle a\rangle+}$ (the encapsulated counter anion is omitted), can be estimated. The time variation of the $\langle a\rangle - \langle c\rangle$ values contains the information about the self-assembly process. To discuss the self-assembly processes more clearly, the $\langle n\rangle$ and $\langle k\rangle$ values, which are derived from the $\langle a\rangle - \langle c\rangle$ values ($\langle n\rangle = (4\langle a\rangle - \langle c\rangle)/\langle b\rangle$, $\langle k\rangle = \langle a\rangle/\langle b\rangle$), are introduced. The $\langle n\rangle$ value indicates the average number of Pd(II) ions binding to a single ditopic ligand **1**, while the $\langle k\rangle$ value the stoichiometric ratio of the Pd(II) ions to **1** in $[Pd_{\langle a\rangle}\mathbf{1}_{\langle b\rangle}X_{\langle c\rangle}]^{2\langle a\rangle+}$.

In this research, 3-chloropyridine (Py*), whose coordination ability is weaker than that of the ditopic ligand **1**, was used as the leaving ligand, X. The self-assembly of the cage was carried out from **1** and $[PdPy^*_4]Y_2$ (Y = BF_4 or OTf) in CD_3NO_2 and CD_2Cl_2 (4:1, v/v) at 298 K and monitored by ^{1}H NMR spectroscopy (Figures 3, S8, and S9). It was found that in the presence of BF_4^- or OTf^-, the cage was formed at 298 K to afford the $(Y^-)\subset[Pd_2\mathbf{1}_4]^{4+}$ cages in 97% (Y = BF_4) and 76% (Y = OTf) yields, which are similar to those found in the self-assembly carried out from **1** and $[Pd(CH_3CN)_4]Y_2$ at 343 K (99% (Y = BF_4) and 62% (Y = OTf)). On the other hand, when a larger counter anion than the size of the cavity of the $[Pd_2\mathbf{1}_4]^{4+}$ cage, BArF (tetrakis[3,5-bis(trifluoromethyl)phenyl]borate), was used as the counter anion, a complicated NMR spectrum was obtained (Figure S10a). Three signals assigned to H^a proton in the ditopic ligand **1** were found after the convergence of the reaction. The integration of these signals based on the internal standard indicates that the species observed by ^{1}H NMR spectroscopy are only 37% based on **1** and that 63% of the substrates were converted into species whose ^{1}H NMR signals are not observable. ^{1}H DOSY measurement indicates that the size of the ^{1}H NMR-observable species is similar to the size of the $[Pd_2\mathbf{1}_4]^{4+}$ cage (Figure S11). ESI-TOF mass spectrometry of the reaction mixture after the convergence showed a signal for $[Pd_2\mathbf{1}_4(NO_3)]^{3+}$ at m/z = 468.1 as a major species (Figure S12), with NO_3^- likely derived from the solvent (CH_3NO_2).[9] If the largest H^a signals at 9.65 ppm is assigned to the $[Pd_2\mathbf{1}_4]^{4+}$ cage, the yield of the free cage is 24%. DLS measurement of the reaction mixture indicates the existence of 40-nm-sized species (Figure S13). These results indicate that large species were mainly produced in the self-assembly with $BArF^-$ and that the guest anions are important for the formation of the $[Pd_2\mathbf{1}_4]^{4+}$ cage, which is probably because the $[Pd_2\mathbf{1}_4]^{4+}$ cage without anion in the cavity is significantly destabilized by the electrostatic repulsion between the two Pd(II) ions with a short distance less than 1 nm. This is supported by DFT calculations of the $(BF_4^-)\subset[Pd_2\mathbf{1}_4]^{4+}$ cage and the $[Pd_2\mathbf{1}_4]^{4+}$cage without BF_4^- in the cavity (Figure S14).

Addition of n-BuN_4BF_4 to a reaction mixture of **1** and $[PdPy^*_4](BArF)_2$ after the convergence (1 day) led to the $(BF_4^-)\subset[Pd_2\mathbf{1}_4]^{4+}$ cage at 298 K in 3 h (Figure S10b). These results indicate that the self-assembly pathway largely depends on the counter anion. The counter anion effect on the conversion into the cage was investigated by addition of several anions (Y^- = OTf^-, ClO_4^-, NO_3^-, and PF_6^-) (Table 1 and Figure S10c). The highest yield (92%) was obtained when ClO_4^- was added. The yield of the cage decreased with increase and decrease in the size of the anions, indicating that the size of the guest anion affects the efficiency of the conversion of large species to the cage.

Table 1. The yields of the cage by the addition of n-Bu_4NY in the reaction mixture from $[PdPy^*_4](BArF)_2$ and **1** after 1 day.

Anion (Y^-)	volume / Å^3	Symmetry	Yield / %
NO_3^-	42.2	D_{3h}	85
BF_4^-	50.6	T_d	83
ClO_4^-	59.2	T_d	92
PF_6^-	76.7	O_h	88
OTf^-	89.8	C_{3v}	62

The self-assembly processes of the cages with different counter anions (BF_4^- or OTf^-) were investigated. The changes in the existence ratios of the substrates and the products in the self-assembly of the $(Y^-)\subset[Pd_2\mathbf{1}_4]^{4+}$ cages from **1** and $[PdPy^*_4]Y_2$ (Y = BF_4 or OTf) are shown in Figure 4a and b. The cage formation from $[PdPy^*_4](BF_4)_2$ occurred much faster than from $[PdPy^*_4](OTf)_2$, suggesting that the guest anion strongly trapped in the cage (BF_4^-) does not only increase the yield of the cage (thermodynamic effect) but also accelerates the self-assembly (kinetic effect). The self-assembly processes in both cases were investigated by the n-k analysis (Figure 4c and d). During the self-assembly from $[PdPy^*_4](BF_4)_2$, the ($\langle n\rangle$, $\langle k\rangle$) value started from around (1.7, 0.6) at 5 min, with the decrease of the $\langle k\rangle$ value, finally reaching around (1.75, 0.5) at 20 min. The ($\langle n\rangle$, $\langle k\rangle$) value remained around there until 1 h (Figure 4c). Then the $\langle n\rangle$ value slightly decreased, while the $\langle k\rangle$ value was constant. This result suggests that the ditopic ligand **1** was incorporated in intermediates from 5 to 20 min to form the partial cage structure, $(BF_4^-)\subset[Pd_2\mathbf{1}_4Py^*]^{4+}$, whose ($n$, k) value is (1.75, 0.5). From 20 to 60 min, the ($\langle n\rangle$, $\langle k\rangle$) value remained around (1.75, 0.5), so $(BF_4^-)\subset[Pd_2\mathbf{1}_4Py^*]^{4+}$ was converted to the $(BF_4^-)\subset[Pd_2\mathbf{1}_4]^{4+}$ cage slowly (the rate-determining step) in the self-assembly (Figure 1).[5a] This is because the intermediate and the transition state produced during the ligand exchange in the final step, where one of the two Pd(II) ions adopts five-coordinate geometry, are destabilized by the structural rigidity of ditopic ligand **1**[10] and because the guest anion further rigidifies the structure of the partial cage.

The self-assembly of the $(BF_4^-)\subset[Pd_2\mathbf{1}_4]^{4+}$ cage from $[PdPy^*_4](BF_4)_2$ and **1** was monitored by ESI-TOF mass spectrometry (Figures S15–17 and Table S13). The signals assigned to the cage were observed from 5 min and are the only species observed during the self-assembly. As weak ^{1}H NMR signals for the cage were observed at 5 min, the mass signals would be partly derived from the cage. QASAP suggests the production of $(BF_4^-)\subset[Pd_2\mathbf{1}_4Py^*]^{4+}$ as a main intermediate. In our previous study, it was found that Py*, whose coordination ability is weak,

is dissociated from the Pd(II) center under the ionization condition, so $(BF_4^-)\subset[Pd_2\mathbf{1}_4Py^*]^{4+}$ would also be detected as the cage by the loss of Py* in the mass spectrometer.[8,9]

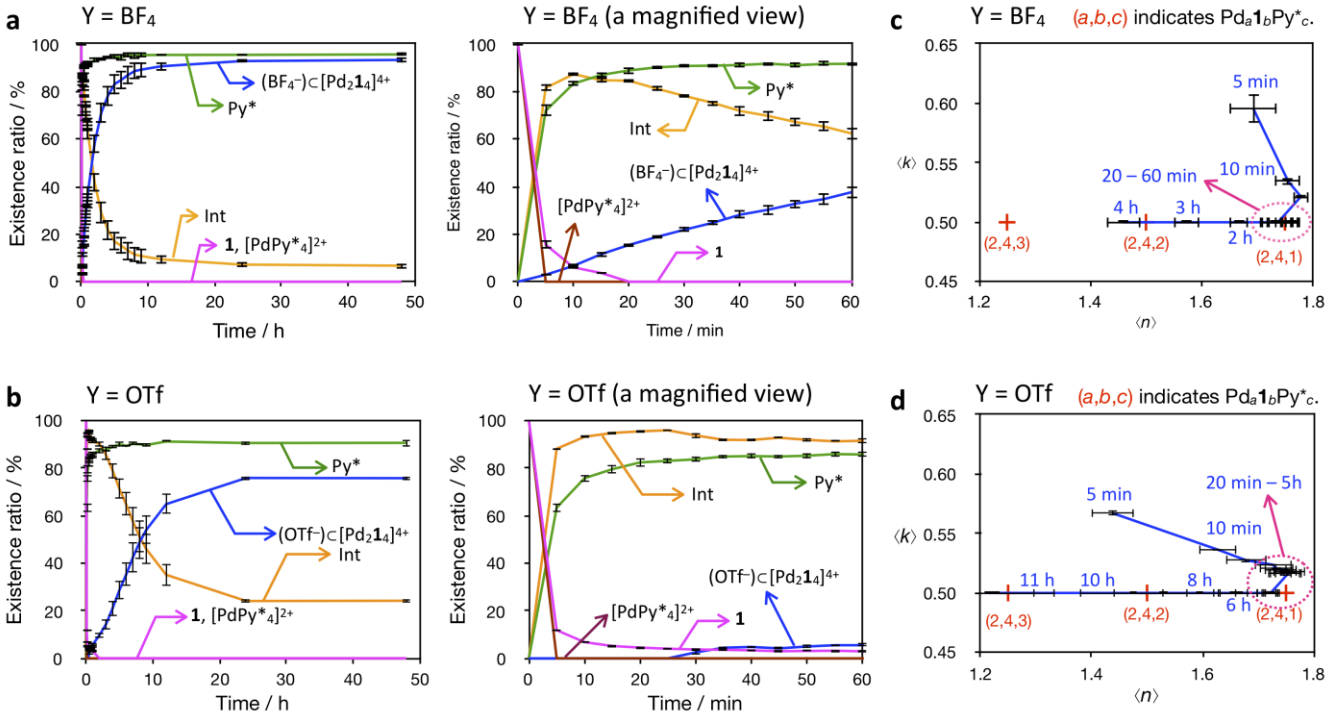

Figure 4. QASAP data for the self-assembly of the $(Y^-)\subset[Pd_2\mathbf{1}_4]^{4+}$ cage from $[PdPy^*_4]Y_2$ (Y = BF_4 or OTf) and **1** in CD_3NO_2 and CD_2Cl_2 (4:1, v/v) at 298 K. (a) and (b) Existence ratios of the substrates and the products for the self-assembly from $[PdPy^*_4](BF_4)_2$ (a) and from $[PdPy^*_4](OTf)_2$ (b). (c) and (d) *n*-*k* plots for the self-assembly from $[PdPy^*_4](BF_4)_2$ (c) and from $[PdPy^*_4](OTf)_2$ (d).

The self-assembly process of the $(OTf^-)\subset[Pd_2\mathbf{1}_4]^{4+}$ cage was investigated by QASAP in the same way. A significant feature of the self-assembly of the $(OTf^-)\subset[Pd_2\mathbf{1}_4]^{4+}$ cage from $[PdPy^*_4](OTf)_2$ and **1** is that the $(OTf^-)\subset[Pd_2\mathbf{1}_4]^{4+}$ cage (54%) was produced without release of Py* after 4 h (Figure 4b). Considering that at least one Py* should be released for the production of one cage from an intermediate composed of no more components than the cage, $[Pd_a\mathbf{1}_bPy^*_c]^{2a+}$ ($a \le 2$, $b \le 4$, $c \ge 1$), the $(OTf^-)\subset[Pd_2\mathbf{1}_4]^{4+}$ cage should be produced from intermediates composed of more components than the cage, $[Pd_a\mathbf{1}_bPy^*_c]^{2a+}$ ($a > 2$, $b > 4$) after 4 h.[9c] The large increase in the $\langle n\rangle$ value with slight decrease in the $\langle k\rangle$ value from 5 to 20 min indicates the growth of intermediates through intra- and intermolecular ligand exchanges during this period to lead to large intermediates. In the case where the $[Pd_2\mathbf{1}_4]^{4+}$ cage is produced by intramolecular ligand exchanges in $[Pd_a\mathbf{1}_bPy^*_c]^{2a+}$ ($a > 2$, $b > 4$) without the release of Py* ($[Pd_a\mathbf{1}_bPy^*_c]^{2a+} \rightarrow [Pd_2\mathbf{1}_4]^{4+} + [Pd_{a-2}\mathbf{1}_{b-4}Py^*_c]^{(2a-4)+}$), the $\langle n\rangle$ value always decreases. As the $(OTf^-)\subset[Pd_2\mathbf{1}_4]^{4+}$ cage was produced with the release of Py* until 4 h, the cage would be formed from the $(OTf^-)\subset[Pd_2\mathbf{1}_4Py^*]^{4+}$ partial cage and from the large intermediates in different pathways.

The self-assembly of the $(OTf^-)\subset[Pd_2\mathbf{1}_4]^{4+}$ cage was monitored by ESI-TOF mass spectrometry (Figures S18–22 and Table S14). Several dinuclear species with 1–5 ditopic ligands were detected during the self-assembly. All the species are considered to be possible intermediates for the cage. However, as all the species appeared during the self-assembly, detailed information about the cage formation process was not gained from the time-dependent mass spectrometry.

To get more detailed information about the self-assembly process on the navigated pathway, NASAP (numerical analysis of self-assembly process)[2g,6] was carried out. In NASAP, the rate constants of the reactions in the reaction network where the possible intermediates that contain no more components than the final assembly ($(Y^-)\subset[Pd_2\mathbf{1}_4]^{4+}$ in this case) are considered (Figure S23) and are numerically determined so that the calculated existence ratios and the ($\langle n\rangle$, $\langle k\rangle$) values well reproduce the corresponding experimental values. QASAP for the self-assembly of the $(BF_4^-)\subset[Pd_2\mathbf{1}_4]^{4+}$ cage suggested that most of the intermediates should contain no more components than the cage, $[Pd_a\mathbf{1}_bPy^*_c]^{2a+}$ ($a \le 2$, $b \le 4$), and that the final step of the self-assembly ($(BF_4^-)\subset[Pd_2\mathbf{1}_4Py^*]^{4+} \rightarrow (BF_4^-)\subset[Pd_2\mathbf{1}_4]^{4+} + Py^*$) is the rate-determining step, so the reaction network where the 25 possible intermediates that are produced by tracking back from the final cage was prepared and total 68 reactions in the network are classified into five types shown in Figure 5a. As QASAP for the $(BF_4^-)\subset[Pd_2\mathbf{1}_4]^{4+}$ cage suggested that the rigidity of dinuclear intermediates would affect the rate of the intramolecular ligand exchanges, the intramolecular reactions are treated separately based on the number of cross-links (Types III–V). A set of rate constants that well reproduces the experimental data (the existence ratios and the ($\langle n\rangle$, $\langle k\rangle$) value with time) was found by master equation approach.

The data set of the rate constants obtained by NASAP (Figure 5e) well reproduces the change in the existence ratios of the substrates and the products (Figure 5b) and captures the trend of the changes in the ($\langle n\rangle$, $\langle k\rangle$) values with time (Figure 5c and d). All the rate constants for backward reaction except for k_{-4} are much smaller than those for the corresponding forward reactions.

Considering that the self-assembly was carried out at mM concentration, the rate for the backward reactions for Type IV is slower than that for the intramolecular forward reactions, even though k_{-4} is larger than k_4. Thus, the backward reactions in the self-assembly of the $(BF_4^-)\subset[Pd_2\mathbf{1}_4]^{4+}$ cage are negligibly slow under this condition (in less coordinative solvent at 298 K). When the rate constants for the intramolecular reactions (k_3, k_4, and k_5) are compared, k_5 ($10^{-1.9}$ min^{-1}) is about one order magnitude smaller than k_3 ($10^{-0.6}$ min^{-1}) and k_4 ($10^{-0.5}$ min^{-1}), which is explained by more rigid structure of the $(BF_4^-)\subset[Pd_2\mathbf{1}_4Py^*]^{4+}$ partial cage, where one of the Pd(II) ions is hard to adopt five-coordination geometry in the transition state of the ligand exchange. The time-course of the main species during the self-assembly suggests the predominant self-assembly pathways (Figure 5e). $[Pd\mathbf{1}Py^*_3]^{2+}$, which is indicated as (1,1,3), is mainly produced and then dinuclear open-chain species ((2,1,6), (2,2,5), (2,3,4), and (2,4,3)) are generated in 1 min. These open structures are cyclized to afford cyclic structures ((2,2,4), (2,3,3), and (2,4,2)) from 1 to 10 min. The second cross-linking (Type IV in Figure 5a) in the cyclic structures yields partial cage structures ((2,3,2) and (2,4,1)) and finally (2,4,1) becomes the dominant intermediate.

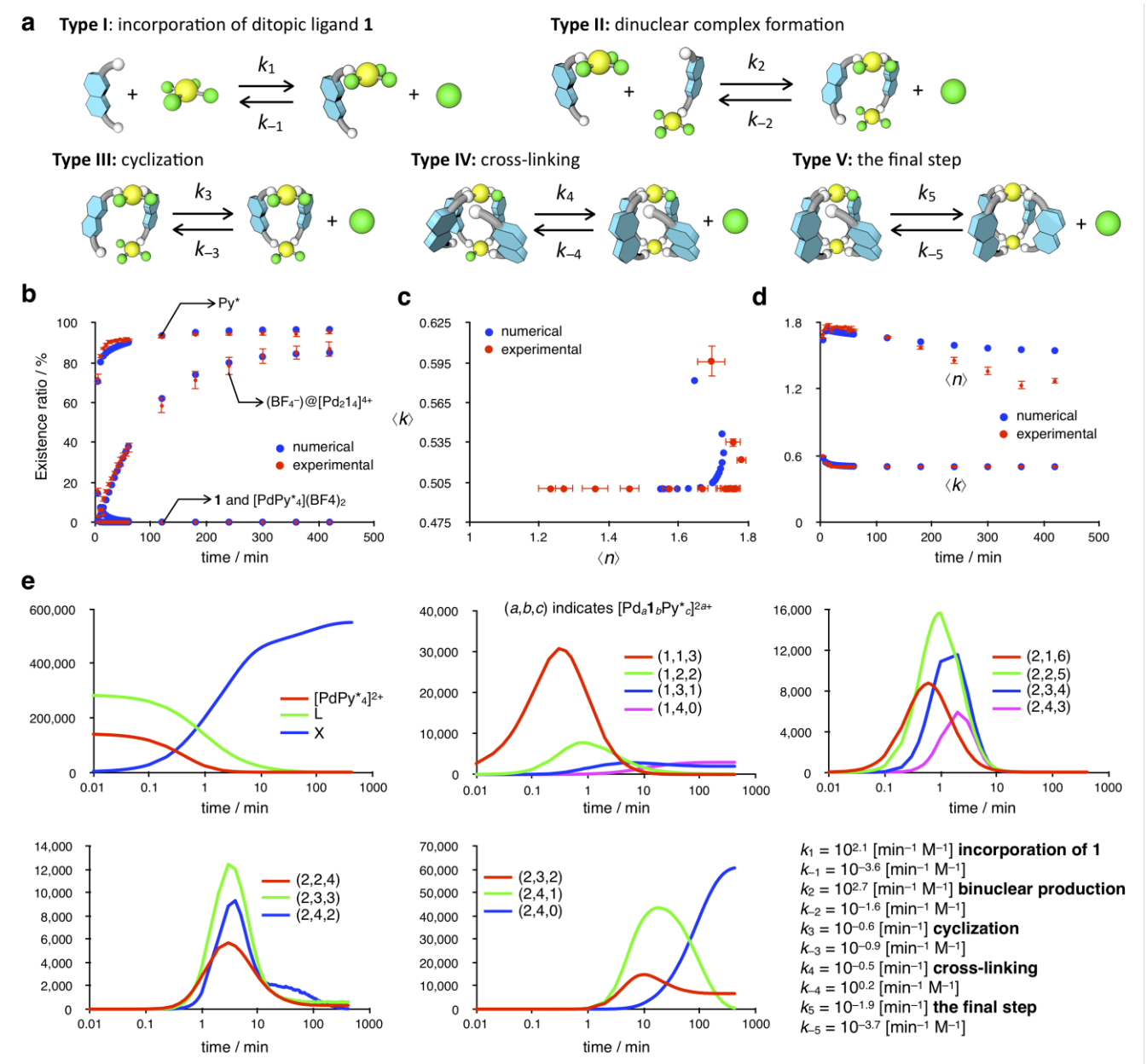

Figure 5. Numerical analysis of self-assembly process (NASAP) of the $(BF_4^-)\subset[Pd_2\mathbf{1}_4]^{4+}$ cage from $[PdPy^*_4](BF_4)_2$ and **1** in CD_3NO_2 and CD_2Cl_2 (4:1, v/v) at 298 K. (a) The five reaction types in the self-assembly of the cage considered in NASAP. Typical examples are shown. The guest anion that would be trapped in between the two Pd(II) ions in the intermediates is omitted. (b) The experimental and numerical data of the existence ratios of the substrates (**1** and $[PdPy^*_4](BF_4)_2$) and the products ($(BF_4^-)\subset[Pd_2\mathbf{1}_4]^{4+}$ and Py*). (c) The experimental and numerical *n*-*k* plots. (d) The changes in the experimental and numerical ⟨*n*⟩ and ⟨*k*⟩ values with time. (e) The time-variation of mainly produced species and a set of the rate constants determined by NASAP.

It was found that the guest anions affect the self-assembly pathway. A good guest anion (BF_4^-), whose binding affinity for the cage is higher than that of OTf^- (confirmed by competition experiments), led the self-assembly along the pathways where

the intermediates are composed of no more components than the cage, while OTf^- could not prevent the transient production of large species because of its weaker template effect. The effect of guest anion found in this study is different from previous examples of template effect in coordination self-assembly. As the $(Y^-)\subset[Pd_2\mathbf{1}_4]^{4+}$ host-guest complex is not energetically most stable, the yield of the cage cannot be improved by simply increasing the thermodynamic stability by encapsulating a good guest anion. A very high yield of the $(BF_4^-)\subset[Pd_2\mathbf{1}_4]^{4+}$ cage (99%) was attained due to kinetic effects, wherein the complementary guest anion promotes selective navigation of the self-assembly pathway thus avoiding the formation of large species. Furthermore, the kinetic stability of the host-guest complex prevents the conversion of the cage to the thermodynamically most stable decomposed state.

CONCLUSIONS

A metastable $(Y^-)\subset[Pd_2\mathbf{1}_4]^{4+}$ cage composed of rigid ditopic ligands **1** and Pd(II) ions was synthesized in very high yield along proper self-assembly pathways navigated by a preferred guest anion (BF_4^-) and little coordinating solvent under kinetic control. The short distance between the two Pd(II) ions in the $[Pd_2\mathbf{1}_4]^{4+}$ cage electrostatically destabilizes the cage without the encapsulated anion, so uncharacterized species, which would be divergent polymeric structures, are produced in the absence of the guest anion. QASAP for the self-assembly of the $(BF_4^-)\subset[Pd_2\mathbf{1}_4]^{4+}$ cage indicates that the intramolecular cross linking in the $(BF_4^-)\subset[Pd_2\mathbf{1}_4Py^*]^{4+}$ partial cage is the rate-determining step, which is supported by NASAP, while intermediates composed of more components than the cage, $[Pd_a\mathbf{1}_bPy^*_c]^{2a+}$ ($a > 2$, $b > 4$), were transiently produced during the self-assembly of the $(OTf^-)\subset[Pd_2\mathbf{1}_4]^{4+}$ cage. Without guest anions ($Y^- = BArF^-$), the self-assembly did not afford the $[Pd_2\mathbf{1}_4]^{4+}$ cage at all and instead produced uncharacterized species, which however can be quickly transformed into the cage by the guest anion (BF_4^-). Considering that these metastable $(Y^-)\subset[Pd_2\mathbf{1}_4]^{4+}$ cages cannot be obtained under usual self-assembly conditions for Pd(II)-linked assemblies (heating in coordinating solvents), the understanding of the self-assembly processes and the knowledge about how to modulate the energy landscape will enable the synthesis of metastable self-assemblies under kinetic control in a rational way.

ASSOCIATED CONTENT

Supporting Information

The Supporting Information is available free of charge on the ACS Publications website.

Synthetic and analytical procedures, analytical data, and NMR spectra (PDF)

Crystallographic data of the $(BF_4^-)\subset[Pd_2\mathbf{1}_4]^{4+}$ cage, CCDC 1940829 (CIF)

AUTHOR INFORMATION

Corresponding Authors

*Paul.Lusby@ed.ac.uk

*chiraoka@mail.ecc.u-tokyo.ac.jp

ORCID

Tomoki Tateishi: 0000-0003-0842-6033

Satoshi Takahashi: 0000-0002-0889-5449

Atsushi Okazawa: 0000-0001-8760-041X

Vicente Martí-Centelles: 0000-0002-9142-9392

Tatsuo Kojima: 0000-0001-7799-8153

Paul J. Lusby: 0000-0001-8418-5687

Hirofumi Sato: 0000-0001-6266-9058

Shuichi Hiraoka: 0000-0002-9262-4747

Notes

The authors declare no competing financial interest.

ACKNOWLEDGMENTS

This work was supported by JSPS KAKENHI Grant Numbers 19H02731, 19K22196, and 19K15531 and The Asahi Glass Foundation and the Leverhulme Trust (V.M.C.; RPG-2015-232).

REFERENCES

(1) (a) Klug, A. The Tobacco Mosaic Virus Particle: Structure and Assembly. *Phil. Trans. R. Soc. Lond.* B **1999**, *354*, 531–535. (b) Williams, R. J.; Smith, A. M.; Collins, R.; Hodson, N.; Das, A. K.; Ulijn R. V. Enzyme-Assisted Self-Assembly under Thermodynamic Control. *Nat. Nanotech.* **2009**, *4*, 19–24. (c) Sharma, J.; Chhabra, R.; Cheng, A.; Brownell, J.; Liu, Y.; Yan, H. Control of Self-Assembly of DNA Tubules Through Integration of Gold Nanoparticles. *Science* **2009**, *323*, 112–116. (d) Chakrabarty, R.; Mukherjee, P. S.; Stang, P. J. Supramolecular Coordination: Self-Assembly of Finite Two- and Three-Dimensional Ensembles. *Chem. Rev.* **2011**, *111*, 6810–6918. (e) Ronson, T. K.; Zarra, S.; Black, S. P.; Nitschke, J. R. Metal–Organic Container Molecules through Subcomponent Self-Assembly. *Chem. Commun.* **2013**, *49*, 2476–2490. (f) Cook, T. R.; Stang, P. J. Recent Developments in the Preparation and Chemistry of Metallacycles and Metallacages via Coordination. *Chem. Rev.* **2015**, *115*, 7001–7045. (g) Wang, W.; Wang, Y.-X.; Yang, H.-B. Supramolecular Transformations within Discrete Coordination-Driven Supramolecular Architectures. *Chem. Soc. Rev.* **2016**, *45*, 2656–2693. (h) Saha, S.; Regeni, I.; Clever, G. H. Structure Relationships between Bis-Monodentate Ligands and Coordination Driven Self-Assemblies. *Coord. Chem. Rev.* **2018**, *374*, 1–14. (i) Zhang, D.; Ronson, T. K.; Nitschke, J. R. Functional Capsules via Subcomponent Self-Assembly. *Acc. Chem. Res.* **2018**, *51*, 2423–2436. (j) De Greef, T. F. A.; Smulders, M. M. J.; Wolffs, M.; Schenning, A. P. H. J.; Sijbesma, R. P.; Meijer, E. W. Supramolecular Polymerization. *Chem. Rev.* **2009**, *109*, 5687–5754. (k) Aida, T.; Meijer, E. W.; Stupp, S. I. Functional Supramolecular Polymers. *Science* **2012**, *335*, 813–817. (l) Sun, H. J.; Zhang, S.; Percec, V. From Structure to Function via Complex Supramolecular Dendrimer Systems. *Chem. Soc. Rev.* **2015**, *44*, 3900–3923. (m) Adelizzi, B.; Aloi, A.; Markvoort, A. J.; Ten Eikelder, H. M. M.; Voets, I. K.; Palmans, A. R. A.; Meijer, E. W. Supramolecular Block Copolymers under Thermodynamic Control. *J. Am. Chem. Soc.* **2018**, *140*, 7168–7175.

(2) (a) Tashiro, S.; Tominaga, M.; Kusukawa, T.; Kawano, M.; Sakamoto, S.; Yamaguchi, K.; Fujita, M. Pd^{II}-Directed Dynamic Assembly of a Dodecapyridine Ligand into End-Capped and Open Tubes: The Importance of Kinetic Control in Self-Assembly. *Angew. Chem. Int. Ed.* **2003**, *42*, 3267–3270. (b) Zheng, Y.-R.; Stang, P. J. Direct and Quantitative Characterization of Dynamic Ligand Exchange between Coordination-Driven Self-Assembled Supramolecular Polygons. *J. Am. Chem. Soc.* **2009**, *131*, 3487–3489. (c) Huang, C.-B.; Xu, L.; Zhu, J.-L.; Wang, Y.-X.; Sun, B.; Li, X.; Yang, H.-B. Real-Time Monitoring the Dynamics of Coordination-Driven Self-Assembly by Fluorescence-Resonance Energy Transfer. *J. Am. Chem. Soc.* **2017**, *139*, 9459–9462. (d) Baba, A.; Kojima, T.; Hiraoka, S. Self-Assembly Process of Dodecanuclear Pt(II)-Linked Cyclic Hexagon. *J. Am. Chem. Soc.* **2015**, *137*, 7664–7667. (e) Tateishi, T.; Kojima, T; Hiraoka, S. Chiral Self-Sorting Process in the Self-Assembly of Homochiral Coordination Cages from Axially Chiral Ligands. *Commun. Chem.* **2018**, *1*, 20. (f) Kai, S.; Kojima, T.; Thorp-Greenwood, F. L.; Hardie, M. J.; Hiraoka, S. How Does Chiral Self-Sorting Take Place in the Formation of Homochiral Pd_6L_8 Capsules Consisting of Cyclotriveratrylene-Based Chiral Tritopic Ligands? *Chem. Sci.* **2018**, *9*, 4104–4108. (g) Komine, S.; Takahashi, S.; Kojima, T.; Sato, H.; Hiraoka, S. Self-Assembly Processes of Octahedron-Shaped Pd_6L_4 Cages. *J. Am. Chem. Soc.* **2019**, *141*, 3178–3186. (h) Tateishi, T.; Yasutake, Y.; Kojima, T.; Takahashi,

S.; Hiraoka, S. Self-assembly Process of a Pd_4L_8 Quadruply Interlocked Cage. *Commun. Chem.* **2019**, *2*, 25.

(3) (a) Hasenknopf, B.; Lehn, J.-M.; Boumediene, N.; Leize, E.; Van Dorsselaer, A. Kinetic and Thermodynamic Control in Self-Assembly: Sequential Formation of Linear and Circular Helicates. *Angew. Chem. Int. Ed.* **1998**, *37*, 3265–3268. (b) Hori, A.; Yamashita, K.; Fujita, M. Kinetic Self-Assembly: Selective Cross-Catenation of Two Sterically Differentiated Pd^{II}-Coordination Rings. *Angew. Chem. Int. Ed.* **2004**, *43*, 5016–5019. (c) Roberts, D. A.; Castilla, A. M.; Ronson, T. K.; Nitschke, J. R. Post-Assembly Modification of Kinetically Metastable $Fe^{II}_2L_3$ Triple Helicates. *J. Am. Chem. Soc.* **2014**, *136*, 8201–8204. (d) Preston, D.; Barnsley, J. E.; Gordon, K. C.; Crowley, J. D. Controlled Formation of Heteroleptic $[Pd_2(L_a)_2(L_b)_2]^{4+}$ Cages. *J. Am. Chem. Soc.* **2016**, *138*, 10578–10585. (e) Burke, M. J.; Nichol, G. S.; Lusby, P. J. Orthogonal Selection and Fixing of Coordination Self-Assembly Pathways for Robust Metallo-Organic Ensemble Construction. *J. Am. Chem. Soc.* **2016**, *138*, 9308–9315. (f) Liu, L.; Lyu, G.; Liu, C.; Jiang, F.; Yuan, D.; Sun, Q.; Zhou, K.; Chen, Q.; Hong, M. Controllable Reassembly of a Dynamic Metallocage: From Thermodynamic Control to Kinetic Control. *Chem. - Eur. J.* **2017**, *23*, 456–461. (g) Ogi, S.; Fukui, T.; Jue, M. L.; Takeuchi, M.; Sugiyasu, K. Kinetic Control over Pathway Complexity in Supramolecular Polymerization through Modulating the Energy Landscape by Rational Molecular Design. *Angew. Chem. Int. Ed.* **2014**, *53*, 14363–14367. (h) Ogi, S.; Stepanenko, V.; Thein, J.; Würthner, F. Impact of Alkyl Spacer Length on Aggregation Pathways in Kinetically Controlled Supramolecular Polymerization. *J. Am. Chem. Soc.* **2016**, *138*, 670–678. (i) Wehner, M.; Röhr, M. I. S.; Bühler, M.; Stepanenko, V.; Wagner, W.; Würthner, F. Supramolecular Polymorphism in One-Dimensional Self-Assembly by Kinetic Pathway Control. *J. Am. Chem. Soc.* **2019**, *141*, 6092–6107.

(4) (a) Schmidt, A.; Casini, A.; Kühn, F. E. Self-Assembled M_2L_4 Coordination Cages: Synthesis and Potential Applications. *Coord. Chem. Rev.* **2014**, *275*, 19–36. (b) Han, M.; Engelhard, D. M.; Clever, G. H. Self-Assembled Coordination Cages Based on Banana-Shaped Ligands. *Chem. Soc. Rev.* **2014**, *43*, 1848–1860. (c) Clever, G. H.; Punt, P. Cation–Anion Arrangement Patterns in Self-Assembled Pd_2L_4 and Pd_4L_8 Coordination Cages. *Acc. Chem. Res.* **2017**, *50*, 2233–2243. (d) Jansze, S. M.; Wise, M. D.; Vologzhanina, A. V.; Scopelliti, R.; Severin, K. $Pd^{II}_2L_4$-Type Coordination Cages up to Three Nanometers in Size. *Chem. Sci.* **2017**, *8*, 1901–1908. (e) Dasary, H.; Jagan, R.; Chand, D. K. Ligand Isomerism in Coordination Cages. *Inorg. Chem.* **2018**, *57*, 12222–12231. (f) Yu, H.-J.; Liu, Z.-M.; Pan, M.; Wu, K.; Wei, Z.-W.; Xu, Y.-W.; Fan, Y.-N.; Wang, H.-P.; Su, C.-Y. Elucidating Anion-Dependent Formation and Conversion of Pd_2L_4 and Pd_3L_6 Metal-Organic Cages by Complementary Techniques. *Eur. J. Inorg. Chem.* **2018**, 80–85. (g) Vasdev, R. A. S.; Gaudin, L. F.; Preston, D.; Jogy, J. P.; Giles, G. I.; Crowley, J. D. Anticancer Activity and Cisplatin Binding Ability of *Bis*-Quinoline and *Bis*-Isoquinoline Derived $[Pd_2L_4]^{4+}$ Metallosupramolecular Cages. *Front. Chem.* **2018**, *6*, 563. (h) Chen, B.; Holstein, J. J.; Horiuchi, S.; Hiller, W. G.; Clever, G. H. Pd(II) Coordination Sphere Engineering: Pyridine Cages, Quinoline Bowls, and Heteroleptic Pills Binding One or Two Fullerenes. *J. Am. Chem. Soc.* **2019**, *141*, 8907–8913. (i) Dasary, H.; Chand, D. K. Structural and Dynamic Aspects of Palladium(II)-Based Self-Assembled Binuclear Coordination Complexes. *Isr. J. Chem.* **2019**, *59*, 248–256. (j) Matsumoto, K.; Kusaba, S.; Tanaka, Y.; Sei, Y.; Akita, M.; Aritani, K.; Haga, M.; Yoshizawa, M. A Peanut-Shaped Polyaromatic Capsule: Solvent-Dependent Transformation and Electronic Properties of a Non-Contacted Fullerene Dimer. *Angew. Chem. Int. Ed.* **2019**, *58*, 8463–8467. (k) Vasdev, R. A. S.; Findlay, J. A.; Garden, A. L.; Crowley, J. D. Redox Active $[Pd_2L_4]^{4+}$ Cages Constructed from Rotationally Flexible 1,1′-Disubstituted Ferrocene Ligands. *Chem. Commun.* **2019**. *55*, 7506–7509.

(5) (a) Tsujimoto, Y.; Kojima, T.; Hiraoka, S. Rate-Determining Step in the Self-Assembly Process of Supramolecular Coordination Capsules. *Chem. Sci.* **2014**, *5*, 4167–4172. (b) Hiraoka, S. What Do We Learn from the Molecular Self-Assembly Process? *Chem. Rec.* **2015**, *15*, 1144–1147. (c) Hiraoka, S. Unresolved Issues That Remain in Molecular Self-Assembly. *Bull. Chem. Soc. Jpn.* **2018**, *91*, 957–978. (d) Hiraoka, S. Self-Assembly Processes of Pd(II)- and Pt(II)-Linked Discrete Self-Assemblies Revealed by QASAP. *Isr. J. Chem.* **2019**, *59*, 151–165.

(6) (a) Matsumura, Y.; Hiraoka, S.; Sato, H. A Reaction Model on the Self-Assembly Process of Octahedron-Shaped Coordination Capsules. *Phys. Chem. Chem. Phys.* **2017**, *19*, 20338–20342. (b) Takahashi, S.; Sasaki, Y.; Hiraoka, S.; Sato, H. A Stochastic Model Study on the Self-Assembly Process of a Pd_2L_4 Cage Consisting of Rigid Ditopic Ligands. *Phys. Chem. Chem. Phys.* **2019**, *21*, 6341–6347.

(7) (a) August, D. P.; Nichol, G. S.; Lusby, P. J. Maximizing Coordination Capsule-Guest Polar Interactions in Apolar Solvents Reveals Significant Binding. *Angew. Chem. Int. Ed.* **2016**, *55*, 15022–15026. (b) Marti-Centelles, V.; Lawrence, A. L.; Lusby, P. J. High Activity and Efficient Turnover by a Simple, Self-Assembled "Artificial Diels–Alderase". *J. Am. Chem. Soc.* **2018**, *140*, 2862–2868.

(8) Kai, S.; Sakuma, Y.; Mashiko, T.; Kojima, T.; Tachikawa, M.; Hiraoka, S. The Effect of Solvent and Coordination Environment of Metal Source on the Self-Assembly Pathway of a Pd(II)-Mediated Coordination Capsule. *Inorg. Chem.* **2017**, *56*, 12652–12663.

(9) (a) Kai, S.; Nakagawa, M.; Kojima, T.; Li, X.; Yamashina, M.; Yoshizawa, M.; Hiraoka, S. Self-Assembly Process of a Pd_2L_4 Capsule: Steric Interactions between Neighboring Components Favor the Formation of Large Intermediates. *Chem. Eur. J.* **2018**, *24*, 3965–3969. (b) Tateishi, T.; Kojima, T.; Hiraoka, S. Multiple Pathways in the Self-Assembly Process of a Pd_4L_8 Coordination Tetrahedron. *Inorg. Chem.* **2018**, *57*, 2686–2694. (c) Kai, S.; Maddala, S. P.; Kojima, T.; Akagi, S.; Harano, K.; Nakamura, E.; Hiraoka, S. Flexibility of Components Alters the Self-Assembly Pathway of Pd_2L_4 Coordination Cages. *Dalton Trans.* **2018**, *47*, 3258–3263. (d) Nakagawa, M.; Kai, S.; Kojima, T.; Hiraoka, S. Energy-Landscape-Independent Kinetic Trap of an Incomplete Cage in the Self-Assembly of a Pd_2L_4 Cage. *Chem. Eur. J.* **2018**, *24*, 8804–8808. (e) Tateishi, T.; Kai, S.; Sasaki, Y.; Kojima, T.; Takahashi, S.; Hiraoka, S. Two Dominant Self-Assembly Pathways to a Pd_3L_6 Double-Walled Triangle. *Chem. Commun.* **2018**, *54*, 7758–7761.

(10) Kai, S.; Martí-Centelles, V.; Sakuma, Y.; Mashiko, T.; Kojima, T.; Nagashima, U.; Tachikawa, M.; Lusby, P. J.; Hiraoka, S. Quantitative Analysis of Self-Assembly Process of a Pd_2L_4 Cage Consisting of Rigid Ditopic Ligands. *Chem. - Eur. J.* **2018**, *24*, 663–671.

Table of Contents (TOC)